J. Space Weather Space Clim. 2023, **13**, 4

https://doi.org/10.1051/swsc/2023001

JSWSC

Available online at:
www.swsc-journal.org

TECHNICAL ARTICLE OPEN ACCESS

The effects of solar radio bursts on frequency bands utilised by the aviation industry in Sub-Saharan Africa

Sarah Ruth McKee[1,*], Pierre Johannes Cilliers[1], Stefan Lotz[1], and Christian Monstein[2]

[1] South African National Space Agency, Hermanus, South Africa
[2] IRSOL Istituto Ricerche Solari "Aldo e Cele Daccò", Università della Svizzera Italiana, via Patocchi 57, CH-6605 Locarno, Switzerland

Received 28 November 2021 / Accepted 26 January 2023

Abstract – Solar radio bursts have been associated with a number of disruptions in avionic systems. The objective of this work is to develop solar radio burst interference thresholds which account for the technical specifications of aviation-related instrumentation, instrument operating frequencies as well as industry stipulated error tolerances. Solar radio bursts are suggested to be potentially hazardous when exceeding these calculated thresholds. Particular attention is paid to the radio altimeter, an important component in aviation safety. The thresholds suggested in this work for VHF communication, GPS navigation receivers and radio altimeter frequencies are; 10^2, 10^3, and 10^4 sfu respectively. Solar radio burst interference (for solar radio bursts above 10^4 sfu) is shown to result in large errors (64–251 m) in the altitude estimates for the Frequency Modulated Continuous Waves (FMCW) radio altimeter simulated in this work.

Keywords: Solar Radio Bursts / Radio altimeter / Space weather effects on aviation

1 Introduction

Solar Radio Bursts (SRBs) are intense radio emissions from the Sun. The intensity of these emissions is elevated above the solar radio emission background. Solar radio emissions are characteristic signatures of solar flares and CME activity. The mechanism for the formation of an SRB can be deduced from its spectral characteristics and frequency range. Table 1 displays different solar radio burst classes and their associated origin mechanisms on the Sun.

SRBs are space weather phenomena that are of great relevance to the avionics industry. These intense radio emissions are capable of causing interference in various radio bands used for navigation and communication purposes in the aviation industry. Solar radio burst interference has the effect of degrading the carrier-to-noise ratio in GPS devices see; Afraimovich et al. (2008), Cerruti et al. (2006), Sreeja et al. (2013, 2014). Secondary air-traffic control ground radar disruptions in Europe on 2015-11-04 were attributed to solar radio burst interference in the L-band (Marqué et al., 2018). Additionally, disturbances in Greenland on this day at the time of the solar radio burst were also reported (Marqué et al., 2018). The ILS (Instrument Landing System) and autopilot systems (operating at VHF frequencies (30–300 MHz)) returned conflicting positioning reports (Marqué et al., 2018). Instrument defects were ruled out post-landing; the incoherent position estimations of the different systems were credited to the solar radio burst interference (Marqué et al., 2018). Solar radio burst interference was shown to be the cause of military operation disruptions during the series of solar flares of May 1967 (21 May–28 May 1967) (Knipp et al., 2016). It is desirable to know how intense extreme SRB events are, which frequency bands an SRB might affect, and how often are they expected to occur (Afraimovich et al., 2008; Bala et al., 2002; Marqué et al., 2018; Nita et al., 2004; Sreeja et al., 2013).

Solar radio emissions are classified according to their spectral characteristics and associated solar phenomena (White, 2007; Monstein, 2012). The type II, III and IV radio bursts are low frequency (<100 MHz) bursts of most interest to space weather studies and applications because these are associated with CME and solar flare activity (White, 2007). Solar radio burst spectral features may be inspected using the e-Callisto instrumentation network. The Compound Astronomical Low-frequency Low-cost Instrument for Spectroscopy and Transportable Observatory (CALLISTO) has been designed as a low-cost instrument for solar radio burst observations in favour of supporting developing countries as outlined by the framework of IHY2007 (International Heliophysical year). More than 200 instruments have been distributed globally forming the e-Callisto network.[1] About 70 instruments provide data on a regular basis to the central server in Switzerland where they are pre-processed and made available to the public. Currently, several international teams are working on real-time burst

*Corresponding author: smckee@sansa.org.za

[1] International network of solar radio spectrometers, a space weather instrument array. http://e-callisto.org/.

Table 1. The five main classes of SRBs which originate in the same of the solar atmosphere that are associated with geo-effective disturbances known as space weather (White, 2007; Yue et al., 2013).

SRB	Description of spectrum	Duration	Frequency range	Associated origin mechanism
Type I	Short duration enhancements of narrow bandwidth usually appearing in groups.	A few seconds	80–200 MHz	Active regionsEruptive prominences
Type II	Slow drift towards lower frequencies over the duration of the burst. Often accompanied by a harmonic.	3–30 min	20–150 MHz	MHD shocksCMEsProton emission eventsFlares
Type III	Short duration. Quickest frequency drift rate of all metric radio bursts (White, 2007)	1–3 s	10 kHz–1 GHz	Active regionsFlares
Type IV	Moving Stationary Continuum	30 min – 2 h Hours – days 3–45 min	20–400 MHz 20 MHz–2 GHz 25–200 MHz	Flares, proton emissions Eruptive prominences MHD shocks Flares, proton emissions
Type V	Always observed trailing a Type III burst.	1–3 min	10–200 MHz	Active regions, Flares

identification and calibration with the aim of future space weather forecasts.

The first flux density threshold estimate, above which SRBs could degrade the quality of GPS L-band communication and navigation, was published by Klobuchar et al. (1999). In particular, the SRB has the effect of reducing the carrier-to-noise ratio of GPS signals (Cerruti et al., 2006). GPS signal tracking disruption on the sunlit side of the Earth for more than 10 min was reported by Afraimovich et al. (2008) during broadband solar radio bursts on 2006-12-06 and 2006-12-13. The degradation of L-band frequency communication and navigation during an SRB is of primary concern for users of multi-frequency GNSS systems as shown in Sato et al. (2019), who analysed the solar radio burst event that occurred on 2017-09-06. This event was particularly important to review since GNSS ground-based receivers, in the latitude sector 20° N–70° N, observed signal interference. This study was important since it reviewed the effects of solar radio bursts and Extreme-Ultra violet (EUV) radiation on GNSS signals. The proposed threshold value was 4×10^4 sfu (solar flux units) on the L_1 GPS frequency (1.575 GHz), noting additionally that only right-hand circularly polarized radio burst emissions would affect the GPS bands (Afraimovich et al., 2008). Given that this threshold value is large compared to the flux of most SRBs at GPS frequencies (Afraimovich et al., 2008), it was assumed that direct interference from SRBs was not an imminent threat to radio communication and navigation (Afraimovich et al., 2008; Sreeja et al., 2013; Sreeja, 2016). Further research had shown that this assumption was oversimplified since much smaller SRB (1000 sfu) were observed to cause significant GPS signal interference across the day side of the Earth (Chen et al., 2005). Other important solar radio bursts around 1000 sfu which caused noteworthy disruptions of GPS operations are detailed in Sato et al. (2019) and Bala et al. (2002). Kintner et al. (2009) mentioned that the threshold of 1000 sfu in this case is only a lower bound on the total solar radio flux needed to disturb GPS signals. This is because the GPS is shown to respond only to the right-hand circularly polarized radio flux (shown by Cerruti et al. 2006). In other words, the radio flux need only be 1000 sfu in the right-hand circular polarization direction to have an effect on communications. Gary et al. (2004) take 1000 sfu to be the appropriate threshold value in their study of solar radio burst impacts on wireless systems. Cerruti et al. (2006) showed in particular the first observations of GPS carrier-to-noise degradation owing to an SRB event. Afraimovich et al. (2008) showed that for an event on 2006-12-06 (near solar minimum), the entire sunlit side of the Earth was affected by GPS positioning disruptions for 10–15 min. Important to note is that the radio emission is wide-band; this will prove to be a crucial factor.

Chen et al. (2005) found that the existing SRB interference threshold of 4×10^4 solar flux units (sfu) was too high for dual frequency codeless and semi-codeless GPS. This was not an isolated observation; the results in Demyanov et al. (2012), Lanzerotti et al. (2005), Nita et al. (2002), Nita et al. (2004), Yue et al. (2013) suggest that the threshold for SRB interference at GPS frequencies should be around ~10^3 sfu. Bala et al. (2002) analysed data from 1960 to 1999 (solar cycles 19 through 22) and found that SRB of at least 10^3 sfu could occur 10–20 times per year on average. The average occurrence rate of these SRBs is skewed by higher occurrence rates during solar maximum periods (Bala et al., 2002). Marqué et al. (2018) concluded that intense SRB at GPS frequencies other than 1415 MHz could go unnoticed by RSTN (Radio Solar Telescope network) since RSTN receivers only observed one discrete frequency in the GPS L-band. If the radio burst is affecting other important aviation communication frequencies such as 1030 MHz, RSTN would not have observed this. Marqué et al. (2018) suggest therefore the importance of having comprehensive monitoring of all frequency bands which form part of critical air traffic control services. Since SRB interference at GPS frequencies has been extensively covered in literature, the focus of this paper will be on aviation-specific frequency bands other than those used by GPS and include the UHF band (300 MHz–3 GHz).

An important avionic component on board an aircraft is the radio altimeter. This component is used to determine the altitude of the flight and is central to safe landings and departures. Hecht (2011) presents a case study of an altimeter initiated aircraft accident. The equipment failure of the left radio altimeter initiated throttle retardation upon descent. Human error in the reaction to this radio altimeter failure culminated in the loss of 9 passenger lives as well as the injury of 177 passengers. At 1950 ft altitude,

the left radio altimeter presented an incorrect altitude estimation of −8 ft. The exact cause of this erroneous estimate was uncertain (Hecht, 2011). Hecht (2011) remarked that there was limited guidance for pilots as to which radio altimeter estimates should be considered anomalous and thus be reported. Hecht (2011) also noted that these erroneous radio altimeter estimates where not uncommon. Erroneous radio altimeter estimates occurred 148 times in a period of 10 months (Hecht, 2011). Hecht (2011) concludes that in order to reliably use radio altimeter data for critical flight functions the data would require meticulous monitoring and comparison against other measurement sources such as the barometric altimeter. The report by Hecht (2011) speaks to the precarious nature of employing radio altimeters which can present capricious altitude estimates in systems which perform critical flight functions. This scenario has provided considerable motivation for the current work.

In order to make a comprehensive determination of the effect of SRBs on aviation communication and navigation services, access to operational and technical information is paramount (Marqué et al., 2018). It would imply comparing different frequency bands and considering the efficacy of the communications in these bands when being used in aviation applications. It is important to consider the region to which certain technical and operational information is pertinent because aviation technology is not necessarily standardized.

The current work considers aviation in Sub-Saharan Africa (geographically, the area of the continent of Africa that lies south of the Sahara desert). In this work, the following technologies will be under consideration: HF communication (3–30 MHz), GPS, VHF radio beacons and radio altimeters. This work includes the re-evaluation of the HF, VHF (30–300 MHz) and radio altimeter frequencies (4.2–4.5 GHz). The question we aim to answer is: What are the appropriate thresholds for the frequency bands used in these applications? This work attempts to provide an initial estimate of these thresholds, for Sub-Saharan Africa, based on operational and technical knowledge.

The paper is organised as follows: Section 2 introduces and derives interference thresholds in the context of SRB interference mitigation. Section 3 discusses data sources and techniques. Section 4 calculates the interference thresholds for various aviation communication and navigation operational frequency bands. Section 5 introduces the reader to an important aviation measurement component, the radio altimeter. Section 6 presents a simulation of the impact of SRBs on the operation of radio altimeters. A summary and conclusions follow in Section 7.

2 Interference thresholds

In order to ascertain which SRBs are hazardous, it is important to determine the intensity of SRBs and to establish a threshold above which the SRB intensity would be hazardous. This section presents both an approach to calculate the SRB intensity and the derivation of an intensity threshold applicable to radio altimetry.

First, define an equivalent solar radio flux density α (sfu) (called F_{eq} in Gary et al. (2004)), for which the solar radio noise level is equivalent to the thermal noise level (Gary et al., 2004). The equivalent solar radio flux density is given in equation (1):

$$\alpha = \frac{8\pi k_\beta T}{G\lambda^2}, \tag{1}$$

where $k_\beta = 1.38 \times 10^{-23}$ J/K is Boltzmann's constant and λ is the carrier wavelength (m). $T = 273$ K is the ambient temperature when the solar radio noise level equals the thermal noise level, and $G = 10$ dBi is the linear gain of the antenna relative to the gain of an isotropic antenna. Gary et al. (2004) calculate a value of 960 sfu for α in their study, See Annex B for the calculation of this value. Nita et al. (2004) use $\alpha = 960$ to establish a relative solar radio flux density F_T (called F_{TN} in Nita et al., 2004) in solar flux units (sfu) (eq. (2)) which is a function of noise sensitivity as well as the carrier frequency of the device v (GHz). See Appendix A for the derivation of equation (2):

$$F_T = \alpha\eta v^2 \text{ (sfu)}. \tag{2}$$

The parameter η defined by equation (2), is a measure of the degree of sensitivity of the device (Nita et al., 2004). η depends on device-specific values for G and T which are varied in order to model different noise levels.

$$\eta = \left(\frac{T}{273}\right)\left(\frac{10}{G}\right). \tag{3}$$

A device with a higher gain G will have a lower interference threshold. A lower value of η means a lower value of F_T and thus the device will be more susceptible to interference by SRBs. In the same sense, the higher the operational temperature the higher the interference threshold. The antenna gain values and temperature values used as inputs in this work are drawn from operational manuals as well as private communications with aviation industry partners in the study region. More information on the actual values used for calculations will accompany the results in Section 4.

Nita et al. (2004) analysed a set of 412 solar radio burst events over the frequency range of 1.2–18 GHz. These events were recorded during the peak of the 23rd solar cycle. Nita et al. (2004) used equation (3) with $\alpha = 960$ in their study which investigated the possibility of interference of the 412 bursts with radio receiving and radar systems that operate at the frequencies 1.2–18 GHz. Nita et al. (2004) found that there is a small probability for solar interference on systems operating at a frequency larger than 2.6 GHz and with a typical noise floor, but that the probability increases significantly at lower frequencies.

After the interference threshold has been calculated, SRB observations are necessary to determine whether or not the SRBs are intense enough to exceed the interference threshold of different devices. The observed radio bursts which surpass the interference threshold of various devices form an extreme subset of events.

3 Data sources

SRB flux observations from the ground-based observational network, RSTN (Kennewell, 2008), are utilised. The list of SRB events used in the analysis was selected from the part of the GOES Solar Proton Event (SEP) list given at https://umbra.nascom.nasa.gov/SEP/ that spanned solar cycles 23 and 24 (1996–2017). Gopalswamy et al. (2015) showed that in solar cycle 24, more halo Coronal Mass Ejections (CMEs) were recorded than in solar cycle 23 even though the solar sunspot number decreased. Kharayat et al. (2017) studied CMEs

Figure 1. Locations of the four RSTN network nodes. The station codes of the four RSTN locations are as follows: LRM – Learmonth Australia, SAVO – San Vito Italy, SAGA – Sagamore Hill Massachusetts USA, K70L-Kaena Point Hawaii. Data files from an additional older site at Palehua Hawaii are also available. Image retrieved from the NOAA RSTN documentation section at https://www.ngdc.noaa.gov/stp/space-weather/solar-data/solar-features/solar-radio/rstn-1-second/documentation/browse_rstn.jpg.

and the associated solar flares for the years 1997–2014. They showed that halo CMEs are most effective at producing SEPs. Additionally, Scolini et al. (2018) showed that 74% of geo-effective CMEs were associated with major SEPs. Using the SEP events from 1996 to 2017 thus provides a representative sample of extreme space weather events, driven by geo-effective CMEs, during solar cycles 23 and 24. This is by no means an exhaustive list of solar radio burst events. It is a list specific to this application that discusses extreme space weather events.

Giersch et al. (2017) showed that even though solar radio burst event records might be missing, an analysis may still be performed on the data, assuming that both the variation in burst peak flux with frequency for extreme space weather events will be preserved and the occurrence rate with respect to frequency is similar to that of the full extreme radio burst population (that is the burst population having no missing burst records).

For each SEP event listed by GOES, the solar radio flux data are inspected for the presence of any SRB events. The SRB events observed in this process are then cross-checked against the NOAA RSTN radio burst list. This is to ensure that the correct radio burst observation is assigned to each SEP event. If there was no radio burst observed, the corresponding SEP event date is eliminated from the event list.

The RSTN network covers eight discrete frequencies: 245, 410, 610, 1415, 2695, 4995, 8800, and 15,400 MHz. The SRB flux data recorded by RSTN are stored on the NOAA archive at https://www.ngdc.noaa.gov/stp/space-weather/solar-data/solar-features/solar-radio/rstn-1-second/. The RSTN network comprises four official sites across the globe. The locations of the official nodes in the RSTN network are indicated in Figure 1.

The observational data for each SRB event can come from a selection of sites in the network and not necessarily from all of the sites. It is thus important to note the observational coverage[2] of the network at each site when retrieving data. Figure 2 is an example of the data which is recorded by RSTN. The maximum solar radio flux during the SRB was recorded for each frequency. Figure 3 is a distribution of the SRB events analysed in this work. The Complementary Cumulative Distribution Function (CCDF) is used for this plot. The CCDF gives the probability that the SRB flux will exceed a value x.

The CCDF function provides an indication of the range of the observed SRB intensities observed in the data. Most importantly it provides an indication of the likelihood of occurrence of large SRBs ($>10^4$ sfu), which can in turn be used to determine the expected frequency of occurrence. It is clear from Figure 3 that observing an SRB with a flux larger than 10^4 sfu, rapidly becomes less probable with increasing flux. This is in agreement with the very first solar radio burst flux threshold set by Klobuchar et al. (1999).

4 SRBs of interest

The SRBs reported in this section exceed the interference threshold of various devices. Note that in this work the interference threshold is being assumed as a tentative candidate device-specific threshold. Consider Figure 4 which is central to this discussion.

Figure 4 illustrates the subset of radio burst observations which are sufficiently intense to exceed the interference threshold at each discrete frequency (orange shaded region between the solid and dashed green curves). The interference thresholds are calculated using equations (2) and (3) for each discrete frequency marked in Figure 4 on the top axis. The calculation was performed for operational temperatures (ITU, 2014a) in the range of −50° and 70 °C, and for typical antenna gain values between $G = 6.3$ dBi and $G = 15.8$ dBi. The interference threshold value at each discrete value (solid green curve in Figure 4) is used for the lower bound column in Table 2. Nita et al. (2004)

[2] https://www.ngdc.noaa.gov/stp/space-weather/solar-data/solar-features/solar-radio/rstn-1-second/documentation/rstn-seon-usaf_ktegnell_31mar16.pdf.

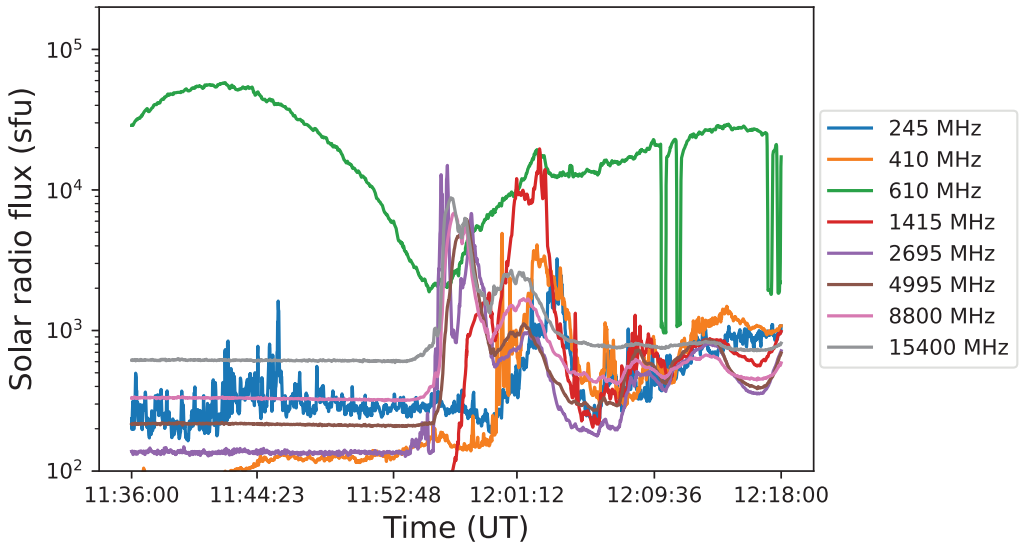

Figure 2. Solar radio flux recorded by RSTN on 2017-09-06 between 11:55 UT and 12:15 UT from RSTN. This data was recorded at the RSTN node in San Vito, Italy. The solar radio burst of interest occurs at 12:00 UT and shows a large enhancement is the microwave band (~1 GHz); the frequencies of which are used for aviation communication and navigation. Sato et al. (2019) investigated the impact this solar radio burst had on GNSS applications. Note that 1 sfu = 10^{-22} W m^{-2} Hz^{-1}.

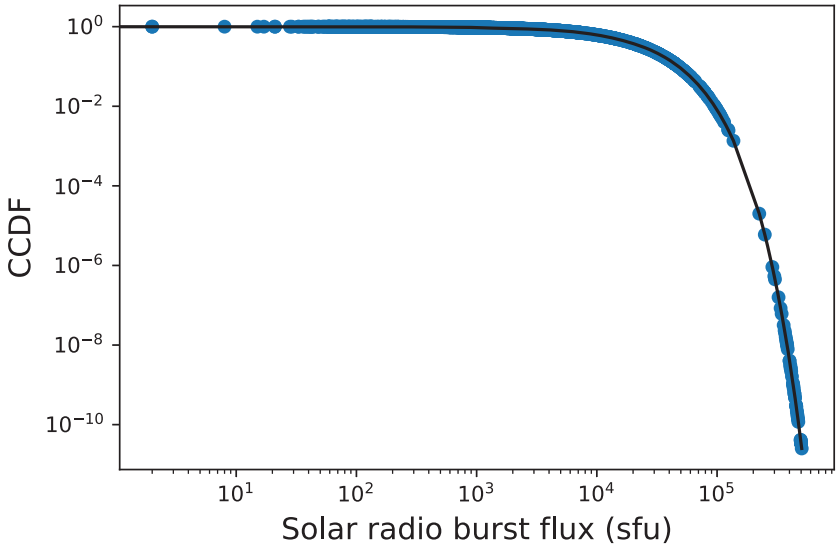

Figure 3. The CCDF of the SRB data set from 1996 to 2017. These events are plotted again in yellow in Figure 4 of Section 4. It is clear that the function is asymptotically decreasing towards 10^6 sfu. Saturation occurs on the RSTN instrument when the flux is larger than 10^6 sfu. There is currently not a global solar radio spectrometer network which is flux calibrated and which can measure above 10^6 sfu.

found that antennas operating in frequency bands above 2.6 GHz are far more resistant to interference from high flux SRBs than devices operating at frequencies lower than 2.6 GHz. They are however not resistant to very extreme events. Based on the data in Figure 4, tentative device-specific thresholds are listed in Table 2.

It is clear from Figure 4 that a solar radio burst exceeding 10^4 sfu may very well be intense enough to disrupt multiple applications simultaneously. This is because for all frequencies less than or equal to 2.6 GHz in Figure 4, a solar radio burst exceeding 10^4 sfu satisfies the condition that the magnitude of the solar radio burst should exceed the interference threshold of the device in order to be of potential harm. This section highlights frequencies less than or equal to 2.6 GHz in particular, since these are the frequencies most commonly affected by solar radio bursts (Nita et al., 2004) and because these are the frequencies that are used for aviation-related communications in the study region. From the work of Nita et al. (2002), there are on average between 9 and 10 events above the threshold expected to occur per year during solar maximum and on average 4.37 events above the threshold per year throughout the course of the solar cycle. As observed by Afraimovich et al. (2008), extreme SRBs are generally broadband phenomena. Multiple frequency blackout is likely in the case of an extreme SRB. Given that HF communication is redundancy built into aviation practices, as well as a mandatory communication during flight

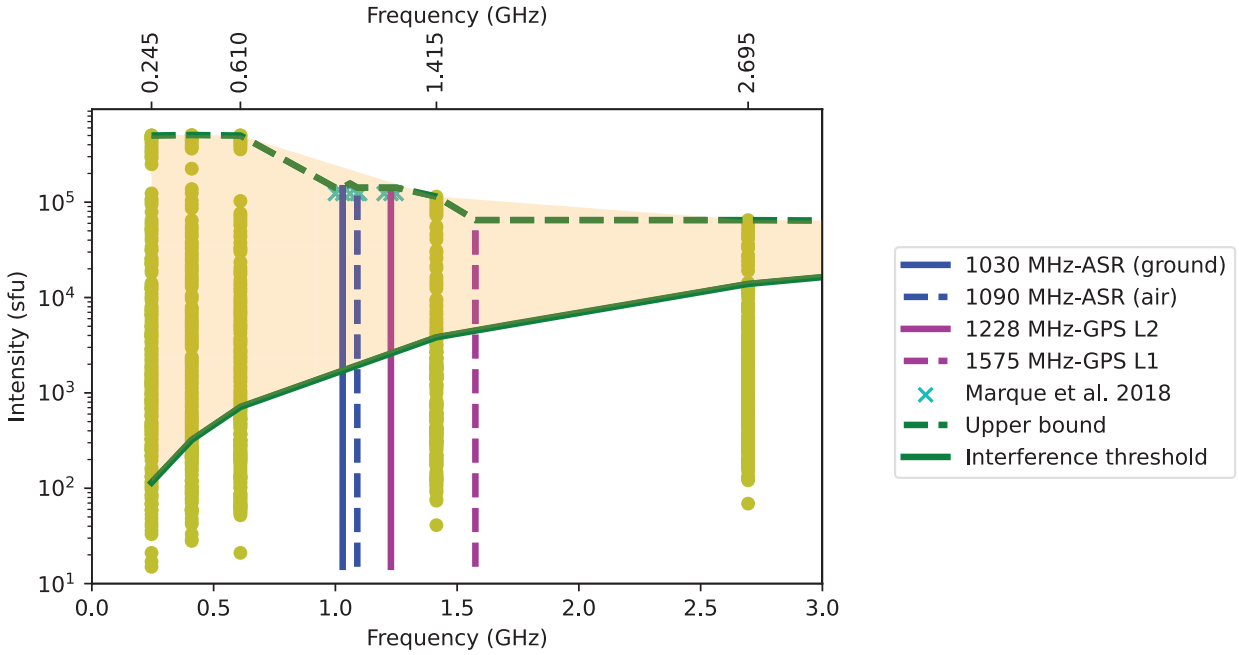

Figure 4. Device-specific thresholds for various aviation-related operational frequencies. RSTN data are marked with yellow dots. The discrete frequencies at which the RSTN data is observed are indicated on the top axis. Data points from observations in Marqué et al. (2018) (cyan x's) at GPS frequencies (1–1.5 GHz) are added. The data from Marqué et al. (2018) consists of e-Callisto data which has been flux-calibrated using data from the ORFEES (Nancay) and HSRS (Humain) observatories. The radar and GPS frequencies which are used in the study region are marked by magenta and dark blue solid and dashed lines. There are no data at these frequencies from the RSTN network. These frequencies can be monitored by using e-Callisto spectral data but no flux-calibrated data is available from e-Callisto for these frequencies. The dashed green curve along the top of the shaded region in Figure 4 is generated by using a cubic spline of the most intense observations at each discrete frequency. The spline values are used for the upper bound column in Table 2.

Table 2. Upper and lower bounds on the SRB flux density. The upper bound is built from a cubic spline of maximum SRB observations. The lower bound is built from equation (2). The magnitudes of SRBs estimated to cause disruption for various instruments are listed alongside the instruments in the table.

Frequency	Lower bound (sfu)	Upper bound (sfu)	Instrumentation	Threshold (sfu)
245 MHz	1.15×10^1	5.00×10^5	HF and VHF	~10^2
410 MHz	3.22×10^2	5.00×10^5		
610 MHz	7.12×10^2	5.00×10^5		
1.03 GHz	2.03×10^3	1.42×10^5	GPS, TACAN and secondary surveillance radar	~10^3
1.06 GHz	2.15×10^3	1.42×10^5		
1.23 GHz	2.88×10^3	1.42×10^5		
1.42 GHz	3.83×10^3	1.14×10^5		
1.58 GHz	4.77×10^3	6.49×10^4		
2.70 GHz	1.39×10^4	6.48×10^4	Primary surveillance radar	~10^4

Civil Aviation Authority (15, April, 2021, A); South African Civil Aviation Authority (25 July 2013), a loss of this mode of communication could pose severe ramifications.

Now that these preliminary thresholds have been posed, a very important avionic component is introduced in the next section. A simulation of the impact of the SRBs on the radio altimeter will follow in Section 6.

5 Importance of radio altimeters

One avionic component for which interference (due to solar radio bursts or otherwise) is unacceptable is the radio altimeter (Flight Safety Foundation, 2000). The radio altimeter operates over the frequencies of 4.2–4.5 GHz. To the knowledge of the authors, there is no literature on the space weather-related impact on radio altimeters. It is however an important instrument for precision landing and in-flight altitude regulation. Radio altimeters form a critical element in the aircraft's Flight Management Guidance Computer (FMGC) and Flight Control systems. Radio altimeters are also critical to the Ground Proximity Warning System (GPWS) or Terrain Avoidance Warning System (TAWS) which are necessary for landing and during low visibility (John, 2011). It is mandatory to have two to three radio altimeters on board so that if one gives a faulty report, the correct altitude can be checked using the other radio altimeters and even the barometric altimeter (given that the barometric altimeter is set correctly (Flight Safety Foundation, 2000)).

Faults within the system will be indicated in the aircraft's Master Minimum Equipment List (MMEL). The systems for which faults are listed in the MMEL may be dispatched (flight allowed to continue) when inoperative if the remaining system configuration allows for safe operation (John, 2011).

Redundancies include VHF emergency frequencies which can be used when there is an unauthorised interception of radio communications (Civil Aviation Authority, 15 April 2021, A; South African Civil Aviation Authority, 25 July 2013). This frequency is used to broadcast distress calls to and from the pilot, to Air Traffic Control (ATC) and surrounding aircraft. If the pilot and ATC can communicate, Air Traffic Navigation Services (ATNS) can recover operations by adapting the original flight plan. This is assuming that the communication frequencies are clear of interference. HF communications are used in cases where there are is operational VHF communication but this is used as a last resort[3] because of frequent noise on HF frequencies.

In case of an altimeter-triggered auto-pilot fault, the pilot needs to undo the system's automated steps and restore the aircraft to manual control (John, 2011; Civil Aviation Authority, 15 April 2021, A; South African Civil Aviation Authority, 25 July 2013). The pilot needs to manually restore the flight to the original documented flight plan which was submitted to (John, 2011; Civil Aviation Authority, 15 April 2021, A; South African Civil Aviation Authority, 25 July 2013). ATNS will then attempt to maintain the flight as planned (Civil Aviation Authority, 15 April 2021, A; South African Civil Aviation Authority, 25 July 2013).

Considering these redundancies, initially, a radio altimeter fault would not appear of serious concern to pilots. However, in the case where the SRB has also interfered with redundant technologies (such as VHF and HF) and communication channels – the failure of a radio altimeter can be problematic. A faulty radio altimeter predicts erroneous flight altitudes and may trigger a fatal chain of commands in the ILS. Cramer (2013) and John (2011) both explain different scenarios when the radio altimeter is either faulty or out of order during the flight. In the case that the radio altimeter is issuing erroneous altitudes and thus inducing hazardous commands in the autopilot, the autopilot can be disengaged/overridden by the pilot (John, 2011). In the case that this occurs during the approach of landing, and in low visibility, the landing will be deemed a missed approach. Aircraft which have missed approach need to be separated from other traffic to ensure safe passage through the airspace (John, 2011). In the case that a flight sends out a distress call about faults in critical equipment, air traffic will be directed to increase the separation between each aircraft (Civil Aviation Authority, 15 April 2021, A; South African Civil Aviation Authority, 25 July 2013). This ensures that the time margin between proximal aircraft is appropriate so as to allow ATC to take control of an aircraft in distress and direct it to landing as per the original flight plan (Civil Aviation Authority, 15 April 2021, A; South African Civil Aviation Authority, 25 July 2013).

The disruption of normal radio altimeter operation would be unacceptable irrespective of the phase of the flight (John, 2011). In the case that the radio altimeter experiences severe radio interference and is consequently rendered out of order, the height above the ground is not determinable. There is a barometric altitude sensor on board but this gives the altitude above sea level and not above the ground. The loss of the radio altimeter measurement means the loss of local terrain height estimates (Cramer, 2013).

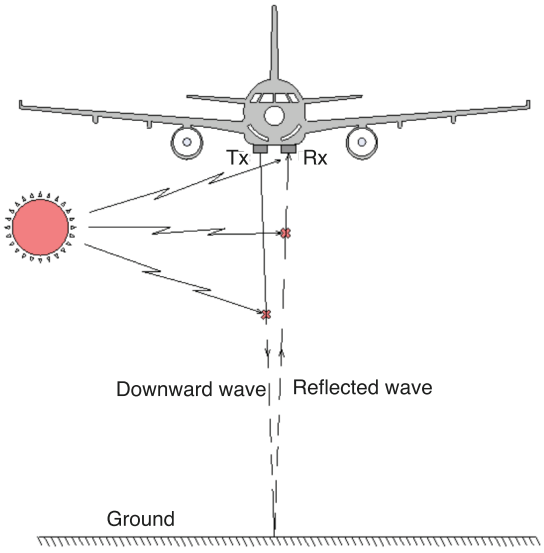

Figure 5. Schematic of the operating principle of a radio altimeter adjusted from (Vidmar, 2006). The red star markers illustrate the solar radio burst interfering with both the downward and the reflected waves before reaching the radio altimeter on-board (transmitter marked with Tx and receiver marked with Rx).

6 Altimeter altitude estimation

In this section, we simulate the impact of SRB interference on the radio altimeter with the aim of assessing the suggested threshold of 10^4 sfu posed in Section 4.

In order to simulate the radio altimeter operation, the method in Kurra (2018) is adapted and implemented for the current work. Kurra (2018) stated that sudden bursts of interference cause a considerable error in the estimated altitude. Wideband solar radio bursts that include the frequencies of radio altimeters are likely to present sudden bursts of interference at radio altimeter frequencies that are similar to radio communication bursts. Figure 5 is a schematic of the scenario discussed in this text.

The operation of a radio altimeter was emulated by considering the technical characteristics (e.g. waveform repetition frequency (Hz), altitude measurement range (m)) of different radio altimeters (see (ITU, 2014a) for the technical characteristics of various radio altimeters). A linear frequency-modulated chirp signal (S_{chirp}) is then built according to these technical characteristics. A delay T must be added to the signal to simulate the mechanism of the radio altimeter. Denote the delayed signal by S_{delay}. The in-flight environment was simulated by adding different noise sources to the signal (Kurra, 2018). The different noise sources can be added to either the transmitted signal (S_{chirp}), the delayed signal (S_{delay}) or both. This would simulate

[3] M. Oelofsen (Chief Pilot), personal communication, April 9, 2021.

Table 3. Simulated altimeter chirp signal specifications.

Wave repetition frequency	150 Hz
Chirp bandwidth	132.8 MHz
Nominal center frequency	4300 MHz

Table 4. Technical characteristics of the analogue radio altimeter being emulated in this work, see Table 1 in ITU (2014a).

Maximum antenna gain	10 dBi
Effective area	0.004 m^2
Cable loss	6 Db
Receiver bandwidth (20 dB emission)	170 MHz
Noise figure	6 dB
Reciever sensitivity	≤ -113 dBm

at which point along the propagation of the signal the interference was experienced. Kurra (2018) considers thermal noise as well as signal interference.

A burst of interference could degrade the accuracy of the altitude estimates significantly (Kurra, 2018). The in-flight environment in this simulation thus has two constituents; white noise and SRB interference. Gaussian white noise (S_{noise}) of appropriate magnitude according to the desired signal-to-noise ratio is added to the signal to emulate the thermal noise ($S_{chirp} + S_{noise}$). The power at the receiver level for different radio altimeters is calculated (Marqué et al., 2018) in order to scale the interference corresponding to different SRB magnitudes. The Minimum Detectable Signal (MDS) is taken as a zeroth order estimate of the input interference threshold. Once the noise and SRB interference (S_{SRB}) is added to the chirp signal ($S_{chirp} + S_{noise} + S_{SRB}$), the correlation between the transmitted signal (S_{chirp}) and the delayed signal (S_{delay}) is calculated and the lag at that point is used as the delay in the radio altimeter signal propagation between transmitter, ground and the receiver.

Let S_{chirp} and S_{delay} be two discrete, real-valued signals. The cross-correlation (Gajic, 2003) between these two signals is calculated and the lag at which the correlation between the two signals is the largest in the time delay t_d between the two signals. This delay t_d is then used in the calculation of the altitude using $h = c \times t_d/2$, where c is the speed of light. The technical characteristics of the signal are in Table 3 and the radio altimeter-specific inputs are in Table 4. The simulation was tested for SRBs in the range of 10^0–10^6 sfu.

Table 5 presents the average errors after 1000 runs of the simulation. The errors generated by solar radio bursts of magnitudes larger than 10^4 sfu far surpass the industry tolerance of 0.45 m (1.5 feet) or 2% (ITU, 2014b). These findings are in agreement with the remark made by Kurra (2018) that a burst of interference can produce large errors in altitude estimation. These errors are especially unacceptable since such a large error at landing would greatly reduce the ability to perform a precision landing.

The height errors fall within industry tolerance for SRB intensity below 10^3 sfu. Given the use of intelligent signal processing techniques, such small errors can be filtered out. In order to apply equation (2) to the radio altimeter in this simulation, the calculations presented by Bala et al. (2002) and Gary et al. (2004) were performed for this receiver with specifications indicated in Table 4. The application of equation (2) for this

Table 5. Radio altimeter altitude average errors as a function of SRB magnitude. The error was calculated by subtracting the input height (12 km) from the estimated height given by $h = \frac{c \times t_d}{2}$ (Kurra, 2018). The simulation results presented in this table are plotted in Figure 6.

SRB magnitude (sfu)	Error (m)	Error (ft)
10^1	0.086 ± 0.0019	0.256 ± 0.0056
10^2	0.239 ± 0.0016	0.718 ± 0.0048
10^3	9.467 ± 0.5493	28.40 ± 1.6478
10^4	62.41 ± 2.5927	187.2 ± 7.7781
10^5	135.8 ± 7.3571	407.3 ± 22.071
10^6	251.8 ± 12.717	755.3 ± 38.153

radio altimeter returns an estimate of 5.73×10^2 sfu for the interference threshold. Note that for this radio altimeter, the bandwidth-dependent value of α in equation (2) becomes 31. Now consider the results in Figure 6, in order to compare this with the simulated errors at each solar radio burst magnitude.

The results in Table 5 confirm that the suggestion of 10^4 sfu as a hazard threshold for radio altimeter frequencies, is appropriate. Firstly, radio bursts with flux at least this large exceed the interference threshold for radio altimeters (Figure 4). Additionally, a solar radio burst flux as large as 10^4 is shown to be capable of causing large radio altimeter errors which are far above industry tolerance (Table 5 indicates this). Additionally, the threshold suggestion of 10^4 sfu is similar to the initial solar radio burst interference threshold estimate of 4×10^4 sfu presented by Klobuchar et al. (1999). At this point, it is important to address possible uncertainties encountered during this study and what impact that might have on the current results. Given that the software and hardware techniques employed by the industry to improve the signal-to-noise ratio are not publicly available, this would imply that the current calculations should be taken as a worst-case scenario of the possible impact of solar radio interference. Nonetheless, it is assumed that the results in this work are representative of the effect of SRB interference on the radio altimeters in sub-Saharan Africa.

The current work provides new information to an important existing niche – the monitoring and maintenance of the efficacy of communication, navigation and altimetry frequency bands used for aviation in Sub-Saharan Africa. These order of magnitude estimates can be implemented as a worst-case reference of solar radio activity levels which can be used to advise the aviation community of potentially hazardous interference on critical frequency bands.

7 Summary and conclusion

A threshold for solar radio interference was first set by Klobuchar et al. (1999). Subsequent to this, various works (Afraimovich et al., 2008; Cerruti et al., 2006; Klein et al., 2018; Marqué et al., 2018; Sato et al., 2019; Sreeja et al., 2013, 2014; Kintner et al., 2009) have shown that this threshold is an overestimate in the case of GPS frequencies. This work addresses the note made by Marqué et al. (2018) that access to more operationally and technically relevant information is required in order to assess the full effect of SRBs. Considering the technologies and measurements available in the study region, this work has presented three conservative preliminary

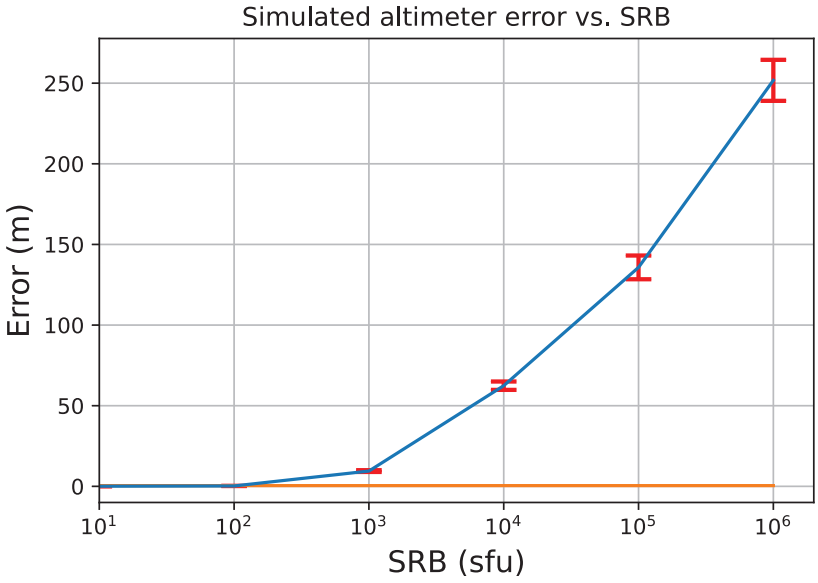

Figure 6. Simulated radio altimeter errors in meters for different solar radio burst magnitudes (sfu), with error bars. If a value of 1 sfu unit is entered into the simulation, it returns a small constant value error estimate of 1.776×10^{-12} m for each iteration. The orange line indicates the industry tolerance.

thresholds which are applicable to HF communication, VHF communication, aircraft monitoring frequencies (GPS and TACAN) and radio altimeters. The calculation of the occurrence frequency of strong radio bursts from the radio burst sample in this work, will be reported in a subsequent research paper. This work contributes to a critical existing niche, the monitoring and maintenance of aviation frequency band efficacy. This work contributes knowledge on how to monitor SRB interference in the study area. This forms part of efforts to mitigate against harmful SRB interference. This work also brings attention to the role of radio altimeters in critical aircraft safety procedures and how solar radio burst interference should be included in the inspection of instrument capabilities.

Acknowledgements. This work is based on research supported wholly by the National Research Foundation of South Africa (Grant Number UID: 127746). The contributions to this work by Chief Pilot Marcel Oelofsen are acknowledged. The authors acknowledge the contribution of Mrs. N Gumede; AFI, RMA(ARMA), ARMA Specialist. The RSTN data were obtained from several USAF stations. The authors acknowledge all of the USAF stations for the use of solar radio data. The authors wish to express their appreciation for the constructive comments provided by the reviewers. Co-Author Monstein thanks the ISSI-Bern International Team of "Why Ionospheric Dynamics and Structure Behave Differently in The African Sector?" (the team leaders E. Yizengaw & K. Groves) for valuable discussion about part of the result that is included in this paper. The editor thanks two anonymous reviewers for their assistance in evaluating this paper.

References

Afraimovich EL, Demyanov VV, Ishin AB, Smolkov GYa. 2008. Powerful solar radio bursts as a global and free tool for testing satellite broadband radio systems, including GPS–GLONASS–GALILEO. *J Atmos Sol Terr Phys* **70**: 1985–1994. http://dx.doi.org/10.1016/j.jastp.2008.09.008.

Bala B, Lanzerotti LJ, Gary DE, Thomson DJ. 2002. Noise in wireless systems produced by solar radio bursts. *Radio Sci* **37**: 2–1. http://dx.doi.org/10.1029/2001RS002481.

Cerruti AP, Kintner PM, Gary DE, Lanzerotti LJ, De Paula ER, Vo HB. 2006. Observed solar radio burst effects on GPS/wide area augmentation system carrier-to-noise ratio. *Space Weather* **4**: 1–9. Article S10006. http://dx.doi.org/10.1029/2006SW000254

Chen Z, Gao Y, Liu Z. 2005. Evaluation of solar radio bursts' effect on GPS receiver signal tracking within International GPS Service network. *Radio Sci* **40**: 1–11. Article RS3012. http://dx.doi.org/10.1029/2004RS003066

Civil Aviation Authority. 15 April 2021. *En-route 0.6-1*, Aeronautical Information Publication.

Civil Aviation Authority. 15 April 2017. *General 0.1-1*, Aeronautical Information Publication.

Cramer J. 2013. *Development of ITU-R Recommendation on Radio Altimeters. ICAO, Aeronautical Communications Panel (ACP) 28th Meeting of working group F.*, Lima, Peru. https://www.icao.int/safety/acp/ACPWGF/ACP-WG-F-28/ACP-WGF28-WP11_Radio%20Altimeter%20input.doc.

Demyanov VV, Afraimovich EL, Jin S. 2012. An evaluation of potential solar radio emission power threat on GPS and GLONASS performance. *GPS Solut* **16**: 411–424. http://dx.doi.org/10.1007/s10291-011-0241-9.

Flight Safety Foundation. 2000. *3.1 – barometric altimeter and radio altimeter. FSF ALAR briefing note*. https://skybrary.aero/bookshelf/books/854.pdf.

Gajic Z. 2003. *Linear dynamic systems and signals*. Prentice Hall/Pearson Education Upper Saddle River.

Gary DE, Lanzerotti LJ, Nita GM, Thomson DJ. 2004. Effects of solar radio bursts on wireless systems. In: *Effects of space weather on technology infrastructure*, Springer, pp. 203–213. http://dx.doi.org/10.1007/1-4020-2754-0_11

Giersch OD, Kennewell J, Lynch M. 2017. Solar radio burst statistics and implications for space weather effects. *Space Weather* **15**: 1511–1522. http://dx.doi.org/10.1002.2017SW001658.

Gopalswamy N, Xie H, Akiyama S, Mäkelä P, Yashiro S, Michalek G. 2015. The peculiar behavior of halo coronal mass ejections in solar cycle 24. *Astrophys J Lett* **804(1)**: L23. http://dx.doi.org/10.1088/2041-8205/804/1/L23.

Hecht H. 2011. So much to learn from one accident crash of 737 on 25 February 2009. In: *2011 IEEE 13th International Symposium on High-Assurance Systems Engineering*, IEEE, pp. 348–351. http://dx.doi.org/10.1109/HASE.2011.4.

ITU. 2014a. *Operational and technical characteristics and protection criteria of radio altimeters utilizing the band 4200–4400 MHz*. International Telecommunications Union, Geneva. https://www.itu.int/dms_pubrec/itu-r/rec/m/R-REC-M.2059-0-201402-I!!PDF-E.pdf.

ITU. 2014b. Operational and technical characteristics and protection criteria of radio altimeters utilizing the band 4200–4400 MHz. ITU. https://www.itu.int/rec/R-REC-M.2059/en

John T. 2011. Aircraft operation of radio altimeters (ACP-WGF24/WP09). *Aeronautical communications panel (ACP) 24th meeting of working group F*, ICAO, Paris, France. https://www.icao.int/safety/acp/ACPWGF/ACP-WG-F-24/ACP-WGF24-WP09_Radio%20Altimeter%20operation%20on%20aircraft%20rev1.doc.

Kennewell JA. 2008. *RSTN solar radio telescopes (discrete frequency) and data*. http://www.deepsouthernskies.com/LSO/RSTN.pdf.

Kharayat H, Prasad L, Pokharia M, Bhoj C, Mathpal C. 2017. Study of large solar energetic particle events with halo coronal mass ejections and their associated solar flares. *New Astron* **53**: 44–52. https://www.sciencedirect.com/science/article/pii/S138410761630183X.

Kintner PM, O'Hanlon B, Gary DE, Kintner PMS 2009.Global positioning system and solar radio burst forensics. *Radio Sci* **44**: 1–6. http://dx.doi.org/10.1029.2008RS004039.

Klein KL, Matamoros CS, Zucca P. 2018. Solar radio bursts as a tool for space weather forecasting. *C R Phys* **19**: 36–42. http://dx.doi.org/10.1016/j.crhy.2018.01.005.

Klobuchar JA, Kunches JM, VanDierendonck AJ. 1999. Eye on the ionosphere: potential solar radio burst effects on GPS signal to noise. *GPS Solut* **3**: 69–71. http://dx.doi.org/10.1007/PL00012794.

Knipp DJ, Ramsay AC, Beard ED, Boright AL, Cade WB, et al. 2016. The May 1967 great storm and radio disruption event: Extreme space weather and extraordinary responses. *Space Weather* **14**: 614–633. https://doi.org/10.1002/2016SW001423.

Kurra J. 2018. *Interference mitigation in radio altimeter*. Jyothsna Kurra. Online: https://oaktrust.library.tamu.edu/handle/1969.1/174374?show=full

Lanzerotti LJ, Gary DE, Nita GM, Thomson DJ, Maclennan CG. 2005. Noise in wireless systems from solar radio bursts. *Adv Space Res***36**: 2253–2257. http://dx.doi.org/10.1016/j.asr.2004.04.013.

Marqué C, Klein KL, Monstein C, Opgenoorth H, Pulkkinen A, Buchert S, Krucker S, Van Hoof R, Thulesen P. 2018. Solar radio emission as a disturbance of aeronautical radio navigation. *J Space Weather Space Clim* **8**: A42. http://dx.doi.org/10.1051/swsc/2018029.

Monstein C. 2012. Catalogue of dynamic electromagnetic spectra observed with Callisto and phoenix – 3. *Radio Astronomy: J Soc Amateur Radio Astronomers* **7**: 63–78.

Nita GM, Gary DE, Lanzerotti LJ. 2004. Statistics of solar microwave radio burst spectra with implications for operations of microwave radio systems. *Space Weather* **2**: 1–7. Article S11005. http://dx.doi.org/10.1029/2004SW000090

Nita GM, Gary DE, Lanzerotti LJ, Thomson DJ. 2002. The peak flux distribution of solar radio bursts. *Astrophys J* **570**: 423. http://dx.doi.org/10.1086/339577.

Sato H, Jakowski N, Berdermann J, Jiricka K, Heßelbarth A, Banyś D, Wilken V. 2019. Solar radio burst events on 6 September 2017 and its impact on GNSS Signal Frequencies. *Space Weather* **17**: 816–826. http://dx.doi.org/10.1029/2019SW002198.

Scolini C, Messerotti M, Poedts S, Rodriguez L. 2018. Halo coronal mass ejections during Solar Cycle 24: reconstruction of the global scenario and geoeffectiveness. *J Space Weather Space Clim* **8**: A09. https://doi.org/10.1051/swsc/2017046.

South African Civil Aviation Authority. 25 July 2013. *Filing of flight plans*. Aeronautical Information Circulation 42-1.

Sreeja V. 2016. Impact and mitigation of space weather effects on GNSS receiver performance. *Geosci Lett* **3**: 1–13. https://doi.org/10.1186/s40562-016-0057-0.

Sreeja V, Aquino M, de Jong K. 2013. Impact of the 24 September 2011 solar radio burst on the performance of GNSS receivers. *Space Weather* **11**: 306–312. http://dx.doi.org/10.1002/swe.20057.

Sreeja V, Aquino M, de Jong K, Visser H. 2014. Effect of the 24 September 2011 solar radio burst on precise point positioning service. *Space Weather* **12**: 143–147. http://dx.doi.org/10.1002/2013SW001011.

Vidmar M. 2006. A landing radio altimeter for small aircraft. In *2006 12th International Power Electronics and Motion Control Conference, 2020–2024*. IEEE. https://doi.org/10.1109/EPEPEMC.2006.4778703.

White SM. 2007. Solar radio bursts and space weather. In: *Physics, environmental science*, Citeseer. Corpus ID: 17892175

Yue X, Schreiner WS, Kuo YH, Zhao B, Wan W, Ren Z, Liu L, Wei Y, Lei J, Solomon S, Rocken C. 2013. The effect of solar radio bursts on the GNSS radio occultation signals. *J Geophys Res Space Phys* **118**: 5906–5918. http://dx.doi.org/10.1002/jgra.50525.

Appendix A

Derivation of the relative solar flux density

Given an antenna with incremental temperature range ΔT_A [K] and an effective area A_A [m^2], the flux density S_A of the noise source at an antenna is given in equation (A.1):

$$S_A = \frac{k_\beta \Delta T_A}{A_A}\left[\frac{\mathrm{W}}{\mathrm{m^2 Hz}}\right], \tag{A.1}$$

where k_β is Boltzmann's constant with units $\frac{\mathrm{J}}{\mathrm{K}}$. Solve for k_β in terms of the solar radio flux of an isotropic antenna S_{eq} as defined in Gary et al. (2004), then:

$$k_\beta = \frac{S_{\mathrm{eq}} A_{\mathrm{eq}}}{\Delta T_{\mathrm{eq}}}. \tag{A.2}$$

Substitute equation (A.2) into (A.1) which produces equation (A.3):

$$S_A = \frac{S_{\mathrm{eq}} A_{\mathrm{eq}}}{\Delta T_{\mathrm{eq}}} \frac{\Delta T_A}{A_A}. \tag{A.3}$$

Given that the effective area A of an antenna can be expressed in terms of the gain G of the antenna, see equation (A.4):

$$G = \frac{4\pi A}{\lambda^2}, \tag{A.4}$$

where λ is the wavelength of an incident wave. Make area A the subject of the formula and substitute equation (A.4) into equation (A.3), this produces:

$$S_A = \frac{S_{\text{eq}}\Delta T_A}{\Delta T_{\text{eq}}}\frac{G_{\text{eq}}\lambda_{\text{eq}}^2}{4\pi}\frac{4\pi}{G_A\lambda_A^2}. \tag{A.5}$$

Recall further that wavelength can be rewritten in terms of frequency by $\lambda = \frac{c}{f}$. Substituting for wavelength in equation (A.5) produces:

$$S_A = \frac{S_{\text{eq}}\Delta T_A}{\Delta T_{\text{eq}}}\frac{G_{\text{eq}}c^2}{f_{\text{eq}}^2}\frac{f_A^2}{G_A c^2}. \tag{A.6}$$

From Gary et al. (2004), $\Delta T_{\text{eq}} = 273$ K since Gary et al. (2004) calculate an equivalent flux at this single temperature and at the gain G_{eq} = 10 dBi. Let $\Delta T_A = T$, $G_A = G$ and $f_A = v$ and make the above substitutions into equation (A.6) then:

$$S_A = S_{\text{eq}}\left(\frac{T}{273}\right)\left(\frac{10}{G}\right)\frac{v^2}{f_{\text{eq}}^2}. \tag{A.7}$$

S_{eq} can be calculated using equation (2) in Gary et al. (2004). $S_{\text{eq}} = 960$ sfu (where S_{eq} is called F_{eq} in Gary et al., 2004) but for this work denote S_{eq} by α. Let $\eta = \left(\frac{T}{273}\right)\left(\frac{10}{G}\right)$ and (F_T is called F_{TN} in Nita et al., 2004) then equation (A.7) reduces to equation (A.8):

$$F_T = \alpha\eta\frac{v^2}{f_{\text{eq}}^2}. \tag{A.8}$$

In the specific case that $f_{eq} \sim 1$ GHz as in Gary et al. (2004), equation (A.8) then reduces further to equation (A.9) which results in equation (A.2) in Nita et al. (2004).

$$F_T = \alpha\eta v^2. \tag{A.9}$$

Appendix B

Quantification of the equivalent solar radio flux density

Begin by simplifying the product $k_\beta T$ in equation (1):

$$\begin{aligned} k_\beta T &= 1.381\times10^{-23}\,\text{J/K}\times 273\,\text{K} \\ &= 3.77\times10^{-21}\,\text{J} \\ &= 3.77\times10^{-21}\,\text{Ws} \\ &= 3.77\times10^{-21}\,\frac{\text{W}}{\text{Hz}}. \end{aligned} \tag{B.1}$$

Given that 1 sfu $= 10^{-22}\frac{\text{W}}{\text{m}^2\text{Hz}}$ then $\frac{\text{W}}{\text{Hz}} = 10^{22}$ sfu m^2. Substituting this definition of $\frac{\text{W}}{\text{Hz}}$ into equation (B.1) produces equation (B.2):

$$\begin{aligned} k_\beta T &= 3.77\times10^{-21}\,\frac{\text{W}}{\text{Hz}} \\ &= 3.77\times10^{-21}\times10^{22}\,\text{sfu}\,\text{m}^2 \\ &= 37.7\,\text{sfu}\,\text{m}^2 \\ &\approx 38\,\text{sfu}\,\text{m}^2. \end{aligned} \tag{B.2}$$

Substituting equation (B.2) into equation (1) along with $\lambda^2 \sim 0.1\,\text{m}^2$ and G = 10 produces:

$$\begin{aligned} \alpha &= \frac{8\pi k_\beta T}{G\lambda^2} \\ &= \frac{(8\pi)(38)(\text{sfu})(\text{m}^2)}{(10)(0.1\,\text{m}^2)} \\ &= (304)(\pi)(\text{sfu}) \\ &= 955\,\text{sfu} \\ &\approx 960\,\text{sfu}. \end{aligned} \tag{B.3}$$

Cite this article as: McKee SR, Cilliers PJ, Lotz S & Monstein C 2023. The effects of solar radio bursts on frequency bands utilised by the aviation industry in Sub-Saharan Africa. *J. Space Weather Space Clim.* **13**, 4. https://doi.org/10.1051/swsc/2023001.